Numerical and experimental characterization of rotational floating body drag

Jonah B. Gadasi, Bryson Robertson, Pedro Lomonaco, Barbara Simpson, Akiri Seki, and Arjun Srinivas

Abstract— [1] **Mid-fidelity models have largely underestimated the low-frequency excitation observed in experimental studies of large floating platforms** [1], [2]. **High-fidelity numerical simulations suggest that these underpredictions are largely caused by a mischaracterization of the viscous damping terms.**

This study investigates the impact of the rotational viscous damping terms on floating body motion and hydrodynamic response using mid-fidelity numerical modelling tools. The research included: [i] an experimental component used to derive viscous damping coefficients of a semisubmersible floating offshore wind turbine specimen using free decay tests and [ii] a numerical component used to quantify performance of two WEC-Sim models; one numerical model included only translational viscous damping terms, while the other included both translational and rotational viscous damping terms. While the study focused on a floating offshore wind turbine platform, findings can be generalized to all floating bodies.

The numerical component resulted in three key findings. First, the low-frequency excitation was likely caused by higher-order wave kinematics. Therefore, numerical models governed by linear wave theory may not exhibit the low-frequency excitation observed in experiments. Second, low-frequency excitation can be incorporated into mid-fidelity models using experimental sea surface elevation time series. Experimental sea surface time series represent real physics, unlike simulated time series generated using linear wave theory assumptions. Finally, including rotational viscous damping had minimal impact on translational position response but was crucial for properly characterizing pitch response. The inclusion of rotational viscous damping terms also improved estimates of mooring line tension, because both surge and pitch motions affect mooring line behaviour.

Keywords—**Floating body, laboratory testing, numerical modelling, scaled prototype, viscous drag**

I. Introduction

There has been rapid growth in the global offshore wind sector in recent years. This trend is expected to continue, as globally installed offshore wind is forecasted to increase from 29 GW in 2019 to 1748 GW by 2050 [1]. The increase in forecasted production is leading developers to move further offshore where the wind resource is more abundant. This has led to the increased popularity of floating offshore wind turbines (FOWTs), which can be installed in locations with deeper water depths [3]. These areas may include coastlines with shorter continental shelves or sites farther offshore where the wind speeds are faster. Furthermore, projects capable of moving farther offshore experience less stakeholder pushback and have access to more untapped real-estate [3]. With this increase in demand comes a need for more economically feasible FOWT designs.

Accurate, mid-fidelity numerical simulation tools are needed to efficiently design FOWT. To improve the accuracy and to understand the limitations of common mid-fidelity numerical modelling tools, the International Energy Agency's (IEA) Wind Technology Collaboration Program (TCP) performed a series of test campaigns entitled Offshore Code Comparison, or OC, to characterize the dynamic and highly coupled behaviour of FOWTs [4]. In the OC5 iteration, participants were encouraged to develop mid-fidelity models of a semisubmersible FOWT using their choice of simulation tools and modelling theories. Participant numerical models were then validated against scaled experimental wind and wave excitation tests of a semisubmersible FOWT specimen tested at the Maritime Research Institute Netherlands (MARIN) [3].

Most participant models adequately represented the experimental behaviour in the linear wave frequency

 This paper is based upon work supported by the United States Department of Energy under Award Number DE-EE0008955.

J. G. Gadasi, Pacific Marine Energy Center (PMEC), Oregon State University (OSU), Corvallis, OR 97331 U.S.A. (email: gadasij@oregonstate.edu).

B. Robertson, PMEC/OSU, Corvallis, OR 97331 U.S.A. (email: bryson.robertson@oregonstate.edu).

P. Lomonaco, O. H. Hinsdale Wave Research Laboratory, Oregon State University Corvallis, OR 97331 U.S.A (e-mail: pedro.lomonaco@oregonstate.edu).

B. Simpson, Civil and Environmental Engineering Department, Stanford University, Stanford, CA 94305 U.S.A. (email: bsimpson@stanford.edu).

A. Seki, Civil and Environmental Engineering Department, Stanford University, Stanford, CA 94305 U.S.A. (email: sekia@stanford.edu).

A. Srinivas is with NAUTILUS Floating Solutions, Bizkaia 48160 Spain. (email: arjun.srinivas@nautilusfs.com).

Digital Object Identifier: https://doi.org/10.36688/ewtec-2023-392

region. However, participant models consistently misrepresented the large low-frequency response observed in the scaled experiments, and most numerical models underpredicted the forces at the base of turbine tower base, mooring line tensions, and surge and pitch motions by about 20% [2]. Mid-fidelity simulations of tension leg platforms resulted in similar underpredictions of the low-frequency response [1]. The long surge and pitch natural periods of large floating platforms lie within this low-frequency region. Designs may be inadequate if numerical models are not capable of accurately representing floating platform behaviour and dynamics within this region. Designers currently overdesign their FOWTs to withstand low-frequency forces to compensate for model inaccuracies, increasing FOWT costs.

Experimental and computational fluid dynamic (CFD) simulations suggest that the low-frequency excitation underestimated in mid-fidelity models may partly arise from higher-order wave forces and mischaracterization of the hydrodynamic viscous forces in platform surge, heave, and pitch [5]. Lopez-Pavon et al. found that incorporating 2nd order wave forces in the form of quadratic transfer functions (QTFs) resulted in better, yet still underpredicted, low-frequency platform response [6], suggesting that higher order wave kinematics may contribute to low frequency platform excitation. Li and Bachynski-Polić developed a QTF correction method that improved the hydrodynamic excitation in the low-frequency and linear wave frequency regions in mid-fidelity models [7]. However, the method needs extensive a priori knowledge of the system behaviour to the inform mid-fidelity models via high-fidelity CFD simulations or complex laboratory experiments [7].

Böhm et al. used viscous drag optimization to improve estimates of low-frequency platform response in mid-fidelity models. The study utilized a global pattern search algorithm on experimental data of irregular sea states to optimize the translational drag coefficients [8]. While improvements were exhibited for the low-frequency platform response, the optimization process must be repeated for every sea state of interest. Additionally, no translational drag coefficients were capable of predicting both the optimal heave and pitch responses [8]. Wang et al. also improved estimates of platform motions in mid-fidelity models by implementing a combination of depth dependent translational drag coefficients and weakly nonlinear Froude Krylov and hydrostatic buoyancy forces [9]. Although estimates of platform motions vastly improved, simply tuning a translational drag coefficient could not accurately represent the pitch moment in both the low-frequency and linear wave frequency regions [9].

These studies suggest that translational viscous damping terms may not adequately represent all response quantities of interest, and rotational viscous damping coefficients may be needed to enhance low-frequency excitation in mid-fidelity models [8]. The previous studies defined mid-fidelity numerical simulations with only translational viscous damping coefficients. Srinivas et al. developed a methodology to numerically derive rotational viscous damping coefficients from validated mid-fidelity numerical models implementing only translational viscous damping coefficients [10]. Their results showed that explicitly defining rotational viscous damping coefficients in mid-fidelity models yielded significantly better estimates of tower base forces and platform surge and pitch motions [10]. However, the methodology was purely numerical and had no physical representation.

Based on the literature, there is a need to characterize the viscous hydrodynamic damping of floating bodies to properly represent the low-frequency response exhibited by FOWTs. This study investigates the impact of rotational viscous damping on floating body surge and pitch motions using mid-fidelity numerical modelling tools. Additionally, a simple yet robust methodology is proposed to experimentally derive and numerically implement rotational viscous damping terms within mid-fidelity numerical models. While the focus of this study is on the rotational viscous effects of a FOWT platform, the methodology can be generalized to all floating bodies.

II. HYDRODYNAMIC MODELLING

Hydrodynamic modelling falls into three levels of fidelity. With each level's increase in accuracy, there is a corresponding computational expense. Low-fidelity models use analytical or frequency dependent solutions to estimate floating body behaviour. Assumptions, such as an inviscid and incompressible fluid, are made to simplify calculations [11]. Mid-fidelity hydrodynamic models use multibody dynamic modelling to estimate floating body behaviour in the time-domain. This approach allows for more accurate estimations by supplementing frequency dependent coefficients from a low-fidelity Boundary Element Method (BEM) potential flow solver with additional time domain forces [11]. Mid-fidelity models may also include higher order terms, such as viscous drag. The most accurate hydrodynamic models are high-fidelity models, which utilize computational fluid dynamics (CFD) or smooth particle hydrodynamics (SPH) to solve the Navier-Stokes equation with limited assumptions. Although these models are the most accurate, they are also extremely computationally expensive and unsuitable for long term seasonal or annual type of performance characterizations [11].

Designers utilize various model fidelities depending on the design phase objective. However, mid-fidelity models are commonly favoured during the design phase as they balance accuracy with computational expense. Mid-fidelity models solve Cummins hydrodynamic equation of motion to describe floating body behaviour, see (1) [12].

$$M\ddot{X}(t) = F_{exc}(t) + F_{Rad}(t) + F_{HS}(t) + F_{Visc}(t) + F_{Moor}(t) \quad (1)$$

On the left-hand side is the inertial force, which is the product of the mass matrix, M, and body acceleration vector, $\ddot{X}(t)$. The wave excitation, $F_{Exc}(t)$, wave radiation, $F_{Rad}(t)$, and hydrostatic, $F_{HS}(t)$, forces are calculated using frequency dependent coefficients from BEM solvers [12]. Mooring forces, $F_{Moor}(t)$, are evaluated using a static, quasi-static, or dynamic mooring model. Model accuracy and computational expense increases from static to quasi-static to dynamic mooring line models [11], [12].

Viscous forces, $F_{Visc}(t)$, are not inherently included in potential flow solutions because of the inviscid fluid assumption [10], [13]. As such, they must be included as additional time domain forces within mid-fidelity models. Otherwise, unrealistically large motion amplitudes can occur. Mid-fidelity models may include viscous terms in two ways. The first methodology is the Morison drag element approach. This approach supplements potential flow solutions with the quadratic drag term from Morison's hydrodynamic equation, (2) [14].

$$F_{Visc} = \frac{1}{2}\rho A_c c_d \left(U(t) - \dot{X}(t)\right)\left|U(t) - \dot{X}(t)\right| \quad (2)$$

The viscous force is the product of the fluid density, ρ, the cross-sectional area perpendicular to the flow, A_c, the fluid flow regime dependent nondimensional drag coefficient c_d, and the relative velocity between the fluid velocity, $U(t)$, and body velocity, $\dot{X}(t)$.

Generally, drag forces are calculated as follows. First, the body is discretized into "strips" with their own nodes. Each node is assigned a geometry and c_d. Second, the distributed drag force is calculated at each node via the Morison equation's drag term. Finally, distributed drag loads are integrated across the cross-sectional length to obtain the body's total drag force [12]. While this methodology is commonly utilized in numerical modelling due to its comprehensive calculation of drag forces across the entire body, its implementation is limited to translational degrees of freedom. Normally, it is assumed that rotational viscous terms can be estimated using small, discretized steps with translational drag coefficients to ease calculations. However, translational drag coefficients derived from translational motions may not be suitable for a rotating body experiencing a different fluid flow regime (velocity and direction), resulting in potentially inaccurate predictions [15].

Alternatively, an additional linear/quadratic damping matrix can be used to incorporate viscosity within mid-fidelity models. In this method, 6x6 matrices of prescribed linear, B_{lin}, and quadratic, B_{quad}, dimensional damping coefficients are used to characterize the viscous damping of the entire body in all degrees of freedom [12]. See (3), where $\dot{X}(t)$ is the body's velocity.

$$F_{Visc} = B_{lin}\left(\dot{X}(t)\right) + B_{quad}\left(\dot{X}(t)\right)\left|\dot{X}(t)\right| \quad (3)$$

Including both linear and quadratic matrices allows for further tuning of the viscous behaviour. However, unlike the Morison element approach, the additional damping matrix methodology utilizes the absolute body velocity instead of the relative velocity in the calculations. Furthermore, the viscous force for the entire body is only calculated and applied at a single point globally, instead of integrating pressures across its surface [10], [12].

III. CASE STUDY

Viscosity was included within WEC-Sim numerical models of a case study FOWT using the additional damping matrix methodology described previously. This approach was selected over the Morison element approach because of its capability of including rotational viscous terms. To complement the numerical models, experiments were conducted in the O.H. Hinsdale Wave Research Laboratory's Directional Wave Basin at Oregon State University. Two sea states were selected based on a resource assessment of potential offshore wind deployment locations along the Oregon coast [16], [17]. Wave conditions can be found in TABLE 1. Note, in the irregular wave case, the numerical models generated a sea surface elevation time series, while in the white noise wave case, an experimental sea surface elevation time series was implemented in the numerical simulations.

A. Physical specimen

A 1:50 Froude scaled semisubmersible platform floating offshore wind turbine was fabricated for this project; see Fig. 1. The semisubmersible platform was modelled after the DeepCwind semisubmersible platform and only the tower of the MARIN Stock turbine was constructed [18]. The specimen's model scale structural properties, excluding moorings, is provided in Table 2. A three-point taut mooring line design was implemented to replicate the linear properties of the catenary line design typically used for this platform.

TABLE 1. FULL-SCALE SEA STATE CONDITIONS.

NAME	IRREGULAR	WHITE NOISE
SPECTRUM	PIERSON MOSKOWITZ	WHITE NOISE
$T\ [s]$	14.28	$6\ to\ 26$
$H\ [m]$	5	5

B. Numerical methods

In this study, the mid-fidelity time-domain hydrodynamic solver WEC-Sim [19] was used to characterize the floating body's response. Frequency dependent wave excitation force coefficients, wave radiation force coefficients, and hydrostatic restoring force coefficients were calculated in the Boundary Element Method (BEM) potential flow solver WAMIT [13]. These coefficients were then used as inputs to estimate time-domain forces within WEC-Sim. The dynamic mooring model MoorDyn was implemented within WEC-Sim to

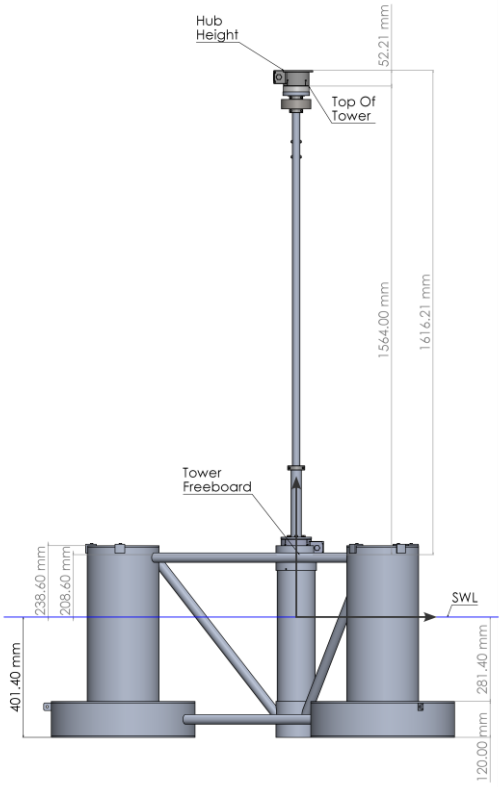

Fig. 1. Model scale semisubmersible platform FOWT.

WIND TURBINE STRUCTURAL PROPERTIES, EXCLUDING MOORINGS.

Parameter	Unit	Model Scale
Total Mass	$[kg]$	111.15
Draft	$[m]$	0.4014
COG along centreline below SWL	$[m]$	0.1609
Roll MI about COG	$[kg\ m^2]$	42.1401
Pitch MI about COG	$[kg\ m^2]$	42.1401
Yaw MI about COG	$[kg\ m^2]$	37.0282

estimate the behaviour of the three-point taut line mooring system [20].

Two separate WEC-Sim models were developed. The first was a "Baseline" model, which only used translation viscous damping coefficients in B_{lin} and B_{quad}. The second was a "Rotational" model, which used both translational and rotational viscous damping terms. Numerical viscous damping coefficients for surge, heave, and pitch were derived from experimental free decay tests performed in the O.H. Hinsdale Directional Wave Basin. Due to 120-degree symmetry, the surge viscous damping coefficients were utilized for sway, and the pitch viscous damping coefficients were utilized for roll. The "Rotational" WEC-Sim model used yaw quadratic viscous damping values from literature of the OC5 DeepCwind semisubmersible [18].

IV. METHODOLOGY

The first step in the hydrodynamic validation campaign was to compare the FOWT's free decay behaviour of both the "Baseline" and Rotational" numerical WEC-Sim models against the experimental results. Once the free decay analysis was performed, the freely floating wave excitation behaviour was examined for the two random wave sea states in Table 1.

A. *System Identification: Free decay*

Free decay tests were used to evaluate the necessary hydrodynamic coefficients. In these tests, the specimen was offset in the desired degree of freedom, released, and allowed to oscillate freely. Mooring line tension and platform surge, heave, and pitch positions were used as metrics for comparing the WEC-Sim models. Tension forces were recorded with inline load cells attached to the end of each mooring line. Positions were measured with the Qualisys motion tracking system.

Body motions, measured via the Qualisys motion tracking system, were used to derive the specimen's natural frequency, linear damping, and quadratic viscous damping coefficients. The natural periods, T_n, were derived using the individual oscillation period zero up-crossing methodology. In this methodology, a new

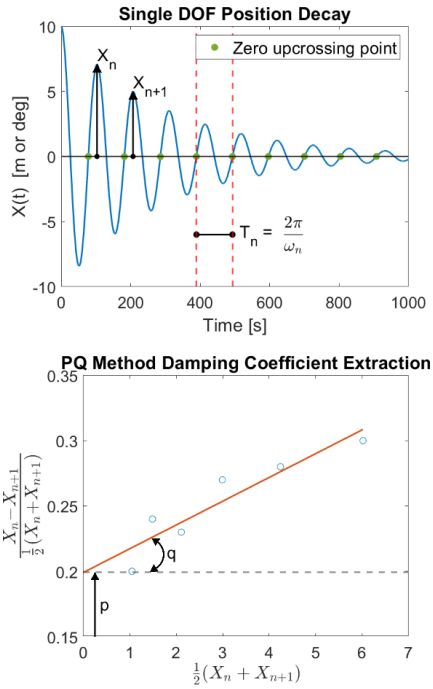

Fig. 2. Representative free decay (a) time series and (b) PQ regression.

oscillation is defined every time the body crosses its "zero" position from negative to positive. This is shown by the circles in the representative decay time series in Fig. 2.(a). The period of each oscillation over the entire time series is averaged to determine the natural period in that degree of freedom.

Linear, B_{lin}, and quadratic, B_{quad}, damping coefficients were derived using the pq methodology [21]. In this method, oscillation amplitudes are used to make a 2D scatter plot, as shown in Fig. 2.(b). The scatter plot's x-axis is the mean between successive crests, while the y-axis is the difference between successive crests divided by their mean. A linear regression line is then fit to the data. The regression line's y-intercept, p, is related to the linear damping coefficient, and its slope, q, is related to the

quadratic damping coefficient by (4) and (5), respectively. In parenthesis is the total mass, given by the summation of the dry mass, M, and the infinite frequency added mass, A_∞.

$$B_{lin} = 2p\frac{M + A_\infty}{T_n} \tag{4}$$

$$B_{quad} = \frac{3}{8}q(M + A_\infty) \tag{5}$$

B. *Hydrodynamic validation*

Power spectral densities (PSD) and PSD sums were used to evaluate the impact that the rotational viscous damping terms have on the low-frequency response. The PSD, or spectral energy distribution of a parameter per unit time, can be defined as the Fourier transform of the autocorrelation function, $R_f(\tau)$ [10], given by $S_f(f)$ in (6). A PSD sum, S_{sum}, allows for the capture of frequency dependent response over a frequency range, and is essentially the integral of the PSD in that region. The equation for the PSD sum of a response across the discrete frequency region from j to k is given by (7), where $S_f(f_i)$ is the discrete PSD of the response at frequency f_i and the frequency increment is Δf.

$$S_f(f) = \int_{-\infty}^{\infty} R_f(\tau)e^{i\omega\tau}d\tau \tag{6}$$

$$S_{sum} = \sum_{i=j}^{k} S_f(f_i)\Delta f \tag{7}$$

The analysis was split into two distinct frequency regions: 1.) the low frequency region from 0.001 Hz to 0.0377 Hz, and 2.) the linear wave excitation region from 0.0385 Hz to 0.2 Hz.

Response amplitude operators (RAOs) were also used to characterize the experimental response of the floating body and compare the numerical models. RAO's are essentially a transfer function that describe the body's behaviour at a particular wave frequency, ω [22].

$$RAO(\omega) = \frac{|\chi|}{a} \tag{8}$$

They are described using (8), where $|\chi|$ is the magnitude of the response and a is the wave amplitude. A white noise wave spectrum was implemented to evaluate the RAOs across a range of frequencies from 6 s to 26 s.

V. RESULTS AND DISCUSSION

A. *System identification: Free decay*

Free decay tests were performed only in surge, heave, and pitch. An overview of the free decay results at full scale is provided in Table 3.

The least squares regression lines derived from each pitch offset's used the least squares averaged [23] p's and q's is provided in Fig. 3. As the colours get warmer, the magnitude of the offset increases. Values of p and q for surge are relatively close for each offset, with p falling between 0.0421 and 0.0678 and q falling between 0.171 and 0.195, the exceptions being the p values for the smallest two offsets, which are noticeably larger. Heave p values have a range between 0.0479 and 0.0671 with an outlier of -0.0183 for the largest amplitude offset. Heave q values lie between 0.187 and 0.275. In pitch, p range from 0.0795 to 0.1341 and q values range from 0.069 to 0.114.

While most of the free decay test pq values from the various offset magnitudes span a reasonable range, the introduction of cross-coupled motion in the experiments introduced some uncertainty. For some trials, a spike in motion was observed after some variable time. This spike was most likely caused by the introduction of another undesired degree of freedom motion exciting the desired degree of freedom. If the entire time series was used in the free decay analysis, results risk contamination as they may no longer represent a single degree of freedom. As such, decay time series were truncated to sections before the

TABLE 3. RESULTS FROM EXPERIMENTAL FREE DECAY TESTS IN THE O.H. HINSDALE DIRECTIONAL WAVE BASIN. ALL RESULTS ARE UPSCALED TO PROTOTYPE SCALE BY FROUDE SCALING.

DoF	NATURAL PERIOD T_n	Linear Damping B_{lin}	Quadratic Damping B_{quad}
Surge	105.85 s	$2.7877e+04\ N\frac{s}{m}$	$1.5027e+06\ N\frac{s^2}{m^2}$
Heave	17.50 s	$1.2399e+05\ N\frac{s}{m}$	$2.2862e+06\ N\frac{s^2}{m^2}$
Pitch	28.11 s	$1.3750e+08\ N\frac{s}{rad}$	$5.5216e+08\ N\frac{s^2}{rad^2}$

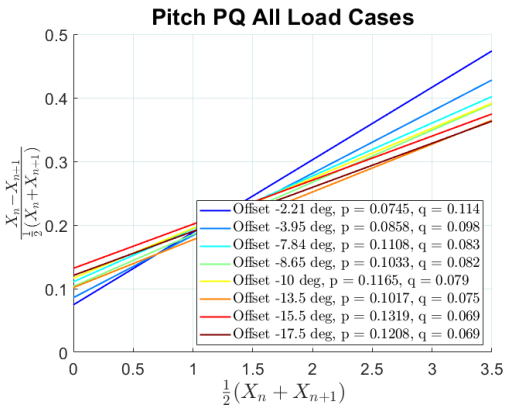

Fig. 3. Pitch linear regression lines for each offset magnitude using trial reweighted averages. The x-axis is the difference between successive decay crests and y-axis is the difference between successive decay crests divided by their mean. The y-intercept is equal to p and the slope is equal to q.

cross-coupled motion was introduced. However, this limited the number of useable peaks available in the pq regression for some trials. Therefore, multiple trials of each offset magnitude were performed to ensure there was enough uncontaminated data.

B. *Hydrodynamic Comparison*

1) *Free decay behaviour*

In the hydrodynamic validation campaign of the mid-fidelity models, the first step compared the free decay behaviour between both the "Baseline" and "Rotational" WEC-Sim models to the experimental results. The surge, heave, and pitch decay timeseries are provided in Fig. 4. An overview of the natural period results for both WEC-Sim models and the experiment can be found in Table 4.

TABLE 4: EXPERIMENTAL, WEC-SIM "BASELINE", AND WEC-SIM "ROTATIONAL" FULL SCALE NATURAL PERIODS FROM FREE DECAY.

DoF	Numerical Natural Period		Experimental Natural Period
	"Baseline"	"Rotational"	
Surge	96.58 *s*	96.65 *s*	105.85 *s*
Heave	17.14 *s*	17.14 *s*	17.50 *s*
Pitch	37.25 *s*	37.27 *s*	28.11 *s*

A comparative analysis of the "Baseline" and "Rotational" WEC-Sim models indicates that the inclusion of rotational viscous terms has a negligible impact on the system's natural frequency, as evidenced by the near-identical natural frequencies observed between the two numerical models for each degree of freedom. Further examination reveals the relative effect of rotational viscous damping terms on the model's motion decay profile. Specifically, the time series of both numerical models show a significant overlap in surge and heave, indicating minimal impact of rotational viscous damping in these degrees of freedom. However, in pitch, the "Baseline" model without rotational viscous terms exhibits essentially undamped motion, while the "Rotational" model displays underdamped pitch decay motion. Notably, the only source of rotational damping in the "Baseline" model comes from radiation damping in the BEM results, which is observed to be negligible based on the "Baseline" model's pitch decay time series. Hence, the inclusion of rotational viscous damping terms is critical in accurately characterizing pitch motion response.

The next step compared the free decay behavior of the numerical WEC-Sim models to the experimental results. In heave, both numerical models aligned well with experimental results; the difference between experimental and numerical heave natural frequencies were negligible, and the heave decay time series was only minimally more damped numerically than experimentally. However, there are some noticeable differences in the surge and pitch decay time series between the numerical simulations and experimental results. In surge, the numerical natural frequencies are about 0.1 Hz larger than the experimental natural frequency. While in pitch the numerical natural

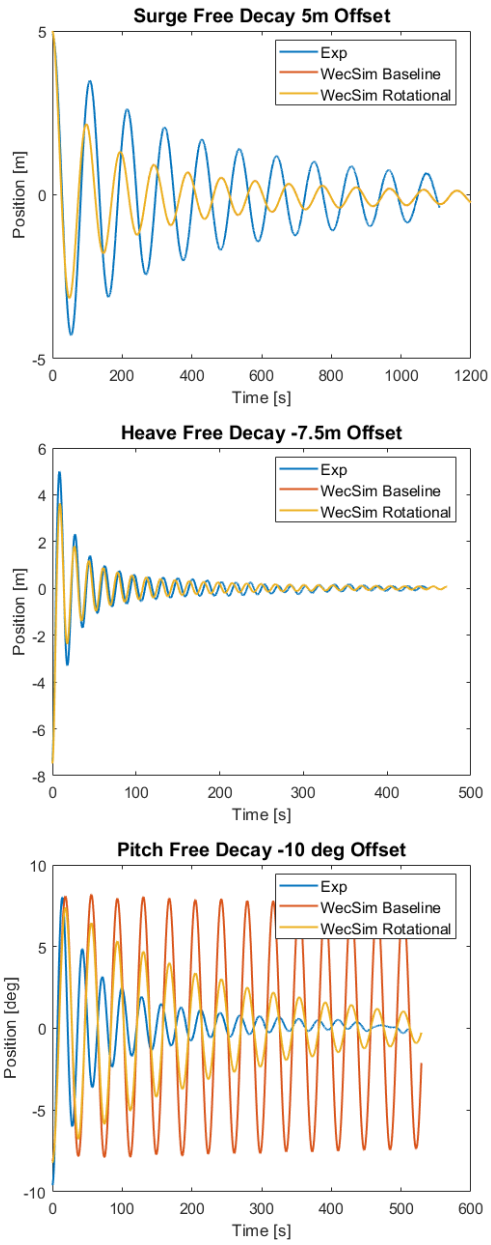

Fig. 4. Full-scale free decay time series for Experimental, WEC-Sim "Baseline", and WEC-Sim "Rotational" viscous damping models. The offsets are (a) $+5\ m$ in surge, (b) $-7.5\ m$ in heave, and (c) $-10°$ in pitch.

frequencies are about 0.1 Hz smaller than the experimental natural frequency. Additionally, the numerical surge and pitch damping behavior varies from the experimental results. In surge, the numerical WEC-Sim models are slightly more damped than the experimental results. While in pitch, the numerical models are less damped than the experimental results.

These discrepancies in surge and pitch decay behavior potentially stem from assumptions about the numerical models' draft. In the WEC-Sim models, the body draft with pretensioned mooring lines was assumed to be the same as the draft without pretensioned mooring lines. Unfortunately, the draft of the system with mooring lines was not recorded, and the small downward pretension force was assumed to result in a small change in draft to reach hydrostatic equilibrium. However, this small change in draft may have led to some unforeseen numerical

consequences. With this assumption in mind, the natural frequency discrepancy between numerical simulations and experimental results can be explained with the equation for damped natural frequency, (9).

$$\omega_d = \sqrt{\frac{k_{tot}}{m_{tot}} - \left(\frac{b_{tot}}{2m_{tot}}\right)^2} \tag{9}$$

Where ω_d is the damped natural frequency, k_{total} is the system's total stiffness, m_{tot} is the system's total mass, and b_{tot} is the system's total damping. In surge, a decreased numerical draft would result in a decreased submerged volume. In turn, this would lead to a smaller surge added mass. Reducing the added mass in the lesser draft numerical models would decrease the total mass, m_{tot}, and yield a larger surge natural frequency numerically than experimentally. In pitch, reducing the draft numerically, while retaining the same center of gravity (COG) and dry mass as the deeper draft experimental setup, would result in a higher numerical center of buoyancy (COB). This yields a numerically smaller metacentric height, which decreases the pitch hydrostatic stiffness in the lesser draft numerical models. A reduction in the pitch hydrostatic stiffness reduces the total stiffness, therefore decreasing the damped pitch natural frequency in the numerical models compared to the experimental results.

The decreased numerical draft assumption may also affect the numerical damping behaviour. In surge, submerged cross-sectional area is directly proportional to the magnitude of the viscous damping coefficients. As the surge cross-sectional area does not change throughout the decay time series, numerical models with less draft implementing experimental surge viscous damping coefficients for a larger draft system would be more damped numerically. In pitch, the total rotational damping force is dependent on the rotational velocity, which is a product of the tangential velocity and the lever arm. For a floating body in WEC-Sim, the lever arm is the metacentric height. Decreasing the draft in the numerical models decreases the lever arm, thereby decreasing the rotational velocity. Implementing the experimental viscous damping coefficients from a system with more draft, while having reduced rotational velocities in the lesser draft numerical models, leads to reduced viscous damping numerically.

2) Free Floating Wave Excitation

The next step compared the wave excitation behaviour of the mid-fidelity WEC-Sim models to the experimental results. PSD plots for the irregular wave case's surge, heave, and pitch positions and up-wave mooring line tension (FAIRTEN2) are provided in Fig. 5. In this study, the up-wave mooring line is defined as the line which experiences the wave first. In the linear wave excitation region, both "Baseline" and "Rotational" numerical models track the experimental results well, aligning with previous studies [2], [5]. A large spike in surge, heave, and mooring line tension response was observed in the numerical models at about $0.0469\ Hz$, which is a harmonic of the larger numerical surge natural frequency. This spike was most likely a numerical error and was possibly due to model aliasing from BEM inputs.

Although both numerical models well estimate the system's linear wave excitation behaviour in the irregular wave case, they largely mischaracterize the low-frequency region behaviour. The low-frequency response is largely underpredicted in surge, heave, and mooring line tension by both the "Baseline" and "Rotational" numerical models. Additionally, there was very little variation between the "Baseline" and "Rotational" numerical models in the low-frequency region for these parameters. The pitch response was poorly represented to varying degrees by the numerical models. Both numerical models displayed a low-frequency pitch resonance condition; however, it occurred at a shorter frequency when compared to the experimental results. This frequency shift aligns with the shorter numerical pitch natural frequency seen in the free decay behaviour analysis. The magnitude of the numerical models' resonance response also differed from the experimental results. The undamped "Baseline" model overpredicted pitch resonance magnitude by about 2.5 times. The "Rotational" model, which was less damped in pitch than the experiment, severely underpredicted the pitch resonance response by about 26 times.

The lack of low-frequency response in the numerical model simulations of the irregular wave case may be due to a potential lack of overall numerical low-frequency excitation. Higher order wave kinematics have been shown to largely contribute to low-frequency excitation in semisubmersible floating offshore wind turbines [5]–[7], [9]. Both WEC-Sim models adhere to linear wave theory assumption, and therefore do not include higher order terms when they simulate the wave field. This may result in a lack of low-frequency surge, heave, and mooring line tension response in both numerical models. In pitch, the low levels of low-frequency excitation near the pitch natural frequency would cause a massive spike in pitch motion response in the undamped "Baseline" model. However, the "Rotational" model with pitch viscous damping would be significantly less sensitive to the low levels of excitation near the pitch natural frequency.

The effect of rotational viscous damping on the system's low-frequency response is further characterized in the PSD sum plots in Fig. 6. The irregular wave case PSD sums for surge position, heave position, pitch position, down-wave mooring line tension (FAIRTEN1), and up-wave mooring line tension (FAIRTEN2) are provided in Fig. 6.(a). Both the "Baseline" and "Rotational" numerical models have smaller irregular wave case PSD sums compared to the experimental results across all parameters. The surge position PSD sum in the "Rotational" model was slightly larger than the "Baseline" model. For the low levels of low-frequency excitation, including rotational viscous damping significantly reduces pitch motion. Therefore, the

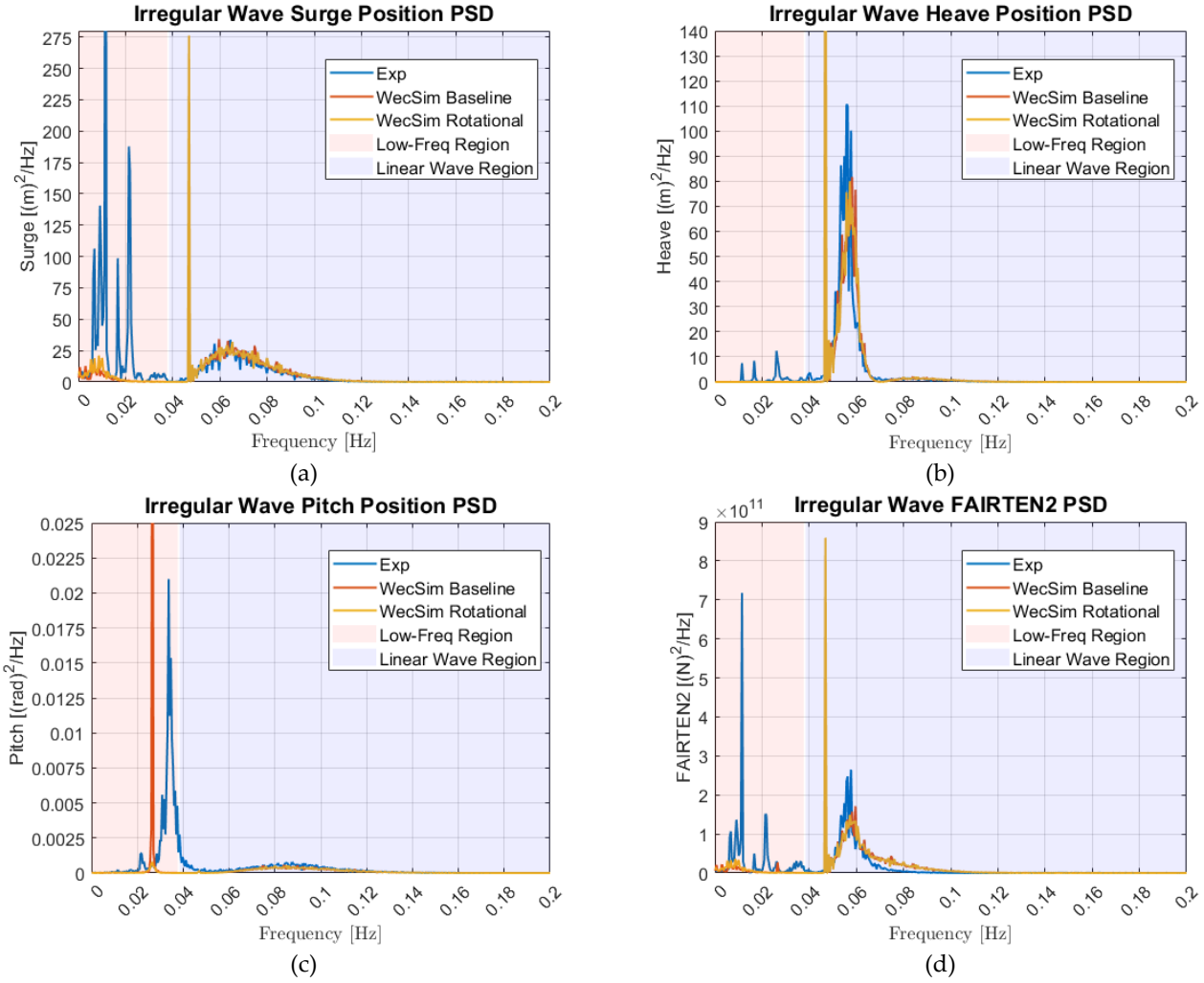

Fig. 5. Free floating wave excitation PSD plots for (a) surge, (b) heave, and (c) pitch platform positions and (d) up-wave mooring line tension (FAIRTEN2) for experimental data and WEC-Sim "Baseline" and "Rotational" model simulations. The sea state is a Pierson Moskowitz spectrum with a $T_p = 14.28\ s$ and $H_{m0} = 5\ m$.

same level of excitation may potentially be expressed more in surge than pitch for the "Rotational" model. Mooring line tension is highly coupled to surge motion, and therefore displays similar results. Irregular wave case low-frequency heave PSD sums were very low in the experimental results. However, both numerical models near zero irregular wave case low-frequency heave PSD sum significantly underpredicts the experiment, further supporting the lack of numerical low-frequency excitation hypothesis. The irregular wave case pitch position PSD sum in the "Baseline" model underpredicted the experimental response by about 2.4 times. This was significantly smaller than the 30 times underprediction observed in the "Rotational" model. However, the "Baseline" model's improved predictions may be because of its unrealistically large sensitivity to small resonance excitation.

The PSD sums for the white noise wave case in Fig. 6 (b) show a different trend than those for the irregular wave case. The white noise wave case surge position PSD sum was still numerically underpredicted, but the inclusion of rotational viscous damping no longer impacts the response. The low-frequency heave position PSD sum of both the "Baseline" and "Rotational" WEC-Sim models were now only slightly less than the experimental results. Unlike the irregular wave case, the pitch position PSD sum for the white noise wave case was larger than the experimental results in both the "Baseline" and "Rotational" numerical models. The undamped "Baseline" model overpredicted the experiment by about 27 times, while the less damped "Rotational" model overpredicted the experiment by 1.5 times.

The numerically overestimated pitch response may be due to the implementation of an experimental sea surface elevation time series in the WEC-Sim simulations. Unlike a numerically simulated sea surface elevation constrained by linear wave theory, an experimental time series is subjected to real world physics. Utilizing experimental elevation time series potentially captured nonlinear wave kinematics, which largely contribute to low-frequency excitation. Therefore, numerical simulations incorporating experimental sea surface elevation time series may react to this introduced low-frequency excitation. The numerical overestimation in the pitch response PSD sum aligns with the numerically less pitch damped system observed in the free decay behaviour analysis. Mooring line tension PSD

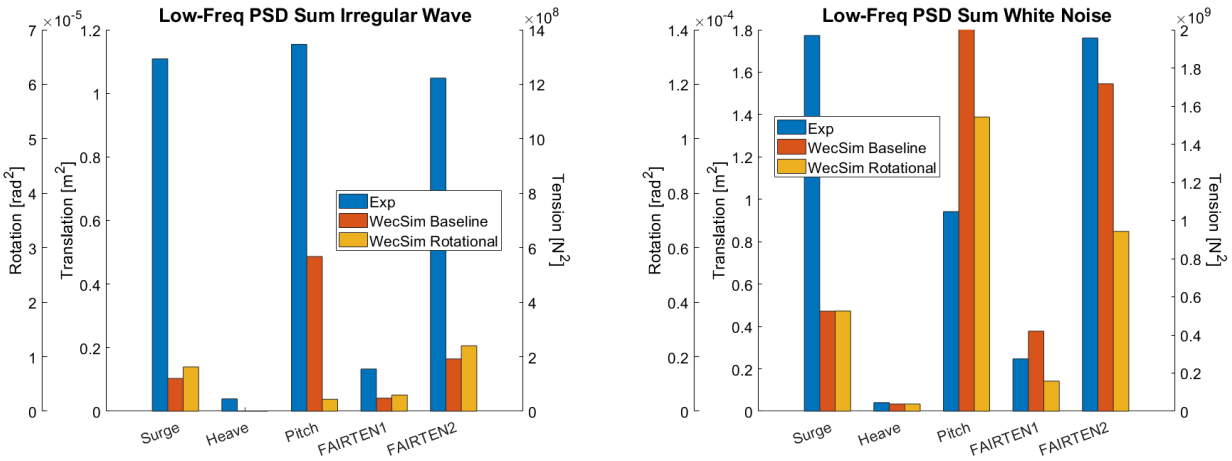

Fig. 6. Low-frequency region PSD sums for surge position, heave position, pitch position, down-wave mooring line tension (FAIRTEN1) and up-wave mooring line tension (FAIRTEN2). (a) irregular wave case with a Pierson Moskowitz spectrum with a $T_p = 14.28\ s$ and $H_{m0} = 5\ m$. (b) white noise wave case with $T = 6\ to\ 26\ s$ and $H = 5\ m$.

sum exhibited improved numerical simulation results when implementing experimental sea surface elevation time series. Pitch motion contributes to the overall mooring line tension. Therefore, improving the pitch motion PSD sum estimations yield better mooring line tension estimations.

The introduction of low-frequency excitation in numerical simulations implementing experimental sea surface elevation time series can be observed in the surge and pitch position white noise wave case RAOs. See Fig. 7, below. The low-frequency surge RAO was unaffected by the inclusion of rotational viscous drag terms, as seen by the overlapping "Baseline" and "Rotational" models. Both numerical models underpredicted the surge resonance response magnitude. However, the numerical models accurately predicted the frequencies of excitation in the low-frequency region. The pitch position low-frequency region resonance condition was once again shifted to a lower frequency in the numerical models, aligning with observations of the free decay behaviour. The numerically overpredicted pitch resonance response magnitude in the white noise RAOs align with numerically less damped behaviour observed in the free decay behaviour analysis. The "Baseline" model overpredicts the experimental pitch position resonance magnitude by about 16.3 times, while the "Rotational" model only overpredicts the experimental results by about 2.5 times.

VI. Conclusion

In conclusion, the hydrodynamic comparison utilizing the mid-fidelity numerical model, WEC-Sim, had three key findings. First, WEC-Sim models assuming linear wave theory exhibited an overall lack of low-frequency excitation observed in experimental wave excitation tests. Nonlinear higher-order wave kinematics are a large contributor to low-frequency excitation in semisubmersible floating offshore wind turbines. Therefore, numerical models governed by linear wave theory intrinsically lack a large portion of low-frequency excitation. This conclusion leads to the second key finding: numerical models implementing experimental sea surface elevation time series exhibit low-frequency excitation. Experimental sea surface elevations are subjected to real world physics and may inherently include nonlinear wave kinematics, unlike sea surface elevations simulated within linearly constrained numerical models. This was seen in the white noise wave case WEC-Sim simulations. Finally, the inclusion of rotational viscous damping had a minimal impact on translational position response but was crucial for properly characterizing pitch response. Additionally, including rotational viscous damping terms improved estimates of mooring line tension, as both surge and pitch motions affect mooring line behavior.

Overall, the hydrodynamic validation campaign highlights the importance of rotational viscous damping in modelling semisubmersible floating offshore wind turbines in mid-fidelity models. Improvements need to be made to the mid-fidelity WEC-Sim models, e.g., models can be run with experimental sea surface elevation time series to represent some of the nonlinear wave dynamics. In the absence of ability to directly include a non-linear force into mid-fidelity models, nonlinear wave dynamics may be included numerically using either 2nd order potential flow quadratic transfer functions (QTFs) from WAMIT's MultiSurf functionality, or through the inclusion of weakly nonlinear Froude Krylov and Hydrostatic Buoyancy terms within WEC-Sim. Additionally, further tuning of the linear and quadratic damping coefficients may improve wave excitation estimates to better match the experimental free decay behaviour.

References

[1] F. Caillé, P. Bozonnet, T. Perdrizet, Y. Poirette, and C. Melis, "MODEL TEST AND SIMULATION COMPARISON FOR AN INCLINED-LEG TLP DEDICATED TO FLOATING WIND," 2017. [Online]. Available: http://asmedigitalcollection.asme.org/OMAE/proceedings-pdf/OMAE2017/57786/V010T09A070/2534888/v010t09a070-

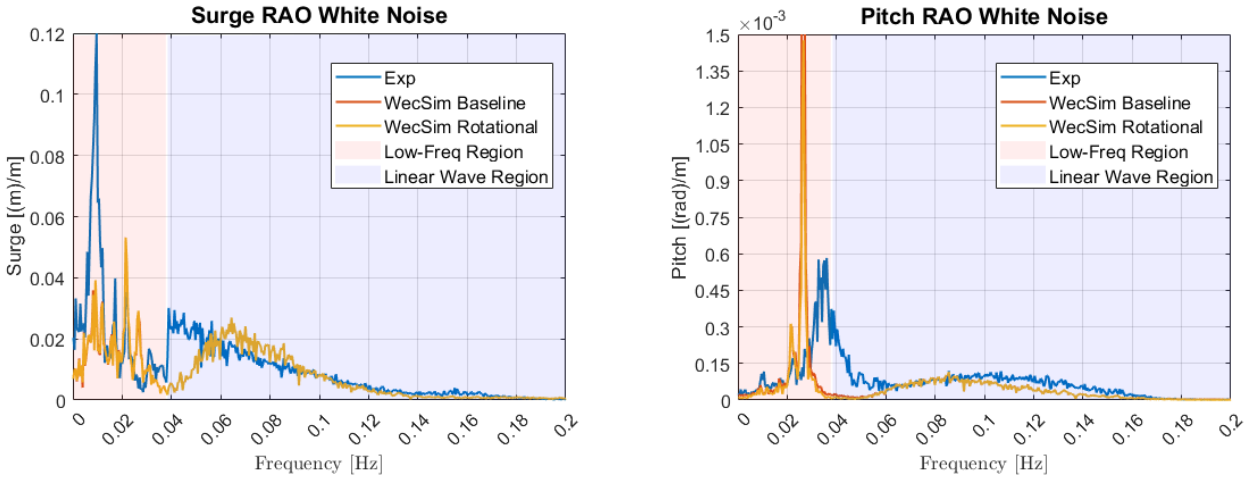

(a) (b)

Fig. 7. (a) surge and (b) pitch position RAOs for the white noise wave case with $T = 6\ to\ 26\ s$ and $H = 5\ m$.

omae2017-61652.pdf

[2] A. N. Robertson *et al.*, "OC5 Project Phase II: Validation of Global Loads of the DeepCwind Floating Semisubmersible Wind Turbine," *Energy Procedia*, vol. 137, pp. 38–57, 2017, doi: 10.1016/j.egypro.2017.10.333.

[3] "FLOATING OFFSHORE WIND: THE NEXT FIVE YEARS," Oslo, Norway, 2022.

[4] International Energy Agency, "IEA Wind TCP Task 30." https://iea-wind.org/task30/ (accessed Feb. 03, 2023).

[5] A. N. Robertson *et al.*, "OC6 Phase I: Investigating the underprediction of low-frequency hydrodynamic loads and responses of a floating wind turbine," in *Journal of Physics: Conference Series*, IOP Publishing Ltd, Sep. 2020. doi: 10.1088/1742-6596/1618/3/032033.

[6] C. Lopez-Pavon, R. A. Watai, F. Ruggeri, A. N. Simos, and A. Souto-Iglesias, "Influence of wave induced second-order forces in semisubmersible fowt mooring design," *J. Offshore Mech. Arct. Eng.*, vol. 137, no. 3, 2015, doi: 10.1115/1.4030241.

[7] H. Li and E. E. Bachynski-Polić, "Analysis of difference-frequency wave loads and quadratic transfer functions on a restrained semi-submersible floating wind turbine," *Ocean Eng.*, vol. 232, Jul. 2021, doi: 10.1016/j.oceaneng.2021.109165.

[8] M. Böhm, A. Robertson, C. Hübler, R. Rolfes, and P. Schaumann, "Optimization-based calibration of hydrodynamic drag coefficients for a semisubmersible platform using experimental data of an irregular sea state," in *Journal of Physics: Conference Series*, IOP Publishing Ltd, Oct. 2020. doi: 10.1088/1742-6596/1669/1/012023.

[9] L. Wang, A. Robertson, J. Jonkman, and Y. H. Yu, "OC6 phase I: Improvements to the OpenFAST predictions of nonlinear, low-frequency responses of a floating offshore wind turbine platform," *Renew. Energy*, vol. 187, pp. 282–301, Mar. 2022, doi: 10.1016/j.renene.2022.01.053.

[10] A. Srinivas, B. Robertson, J. B. Gadasi, B. G. Simpson, P. Lomónaco, and J. M. B. Ilzarbe, "Impact of Limited Degree of Freedom Drag Coefficients on a Floating Offshore Wind Turbine Simulation," *J. Mar. Sci. Eng.*, vol. 11, no. 1, Jan. 2023, doi: 10.3390/jmse11010139.

[11] M. Leary, C. Rusch, Z. Zhang, and B. Robertson, "Comparison and validation of hydrodynamic theories for wave energy converter modelling," *Energies*, vol. 14, no. 13, Jul. 2021, doi: 10.3390/en14133959.

[12] J. B. Gadasi, "Hydrodynamic Characterization of Floating Offshore Wind Turbines: An Experimental and Numerical Multi-Degree of Freedom Analysis," Oregon State University, Corvallis, 2023.

[13] C.-H. Lee and J. N. Newman, "WAMIT." Department of Ocean Engineering, MIT, Boston, MA, 1999. [Online]. Available: https://www.wamit.com/

[14] J. R. Morison, M. P. O'brien, J. W. Johnson, and S. A. Schaaf, "THE FORCE EXERTED BY SURFACE WAVES ON PILES." [Online]. Available: http://onepetro.org/JPT/article-pdf/2/05/149/2238818/spe-950149-g.pdf/1

[15] "ProteusDS Manual." 2018.

[16] B. Robertson, G. Dunkle, J. Gadasi, G. Garcia-Medina, and Z. Yang, "Holistic marine energy resource assessments: A wave and offshore wind perspective of metocean conditions," *Renew. Energy*, vol. 170, pp. 286–301, 2021, doi: 10.1016/j.renene.2021.01.136.

[17] W. D. Musial, P. C. Beiter, J. Nunemaker, D. M. Heimiller, J. Ahmann, and J. Busch, "Oregon Offshore Wind Site Feasibility and Cost Study," no. October, 2019, [Online]. Available: http://www.osti.gov/servlets/purl/1570430/

[18] A. Robertson, J. Jonkman, F. Wendt, A. Goupee, and H. Dagher, "Definition of the OC5 DeepCwind Semisubmersible Floating System." p. 44, 2016.

[19] Y.-H. Yu *et al.*, "WEC-Sim." 2020. doi: 10.5281/zenodo.3924764.

[20] M. Hall, "MoorDyn User's Guide." 2015. [Online]. Available: https://nwtc.nrel.gov/FAST8

[21] J. Helder and Mario Pietersma, "UMaine-DeepCwind/OC4 Semi Floating Wind Turbine Repeat Tests," Wageningen, 2013.

[22] O. M. Faltinsen, *Sea Loads on Ships and Offshore Structures*. Cambridge: Cambridge University Press, 1990.

[23] D. P. O'Leary, "ROBUST REGRESSION COMPUTATION USING ITERATIVELY REWEIGHTED LEAST SQUARES," 1990. [Online]. Available: https://epubs.siam.org/terms-privacy